



HAL
open science

Transformational fluctuation electrodynamics: application to thermal radiation illusion

Ahmed Alwakil, Myriam Zerrad, Michel Bellieud, Denis Veynante, Franck Enguehard, Nathalie Rolland, Sebastian Volz, Claude Amra

► **To cite this version:**

Ahmed Alwakil, Myriam Zerrad, Michel Bellieud, Denis Veynante, Franck Enguehard, et al.. Transformational fluctuation electrodynamics: application to thermal radiation illusion. *Optics Express*, 2017, 25 (15), pp.17343. 10.1364/OE.25.017343 . hal-01565224

HAL Id: hal-01565224

<https://hal.science/hal-01565224>

Submitted on 19 Jul 2017

HAL is a multi-disciplinary open access archive for the deposit and dissemination of scientific research documents, whether they are published or not. The documents may come from teaching and research institutions in France or abroad, or from public or private research centers.

L'archive ouverte pluridisciplinaire **HAL**, est destinée au dépôt et à la diffusion de documents scientifiques de niveau recherche, publiés ou non, émanant des établissements d'enseignement et de recherche français ou étrangers, des laboratoires publics ou privés.

Transformational fluctuation electrodynamics: application to thermal radiation illusion

AHMED ALWAKIL,^{1,*} MYRIAM ZERRAD,¹ MICHEL BELLIEUD,² DENIS VEYNANTE,³ FRANCK ENGUEHARD,³ NATHALIE ROLLAND,⁴ SEBASTIAN VOLZ,^{3,5} AND CLAUDE AMRA¹

¹*Aix Marseille Univ, CNRS, Institut Fresnel, Avenue Escadrille Normandie Niemen, 13397, Marseille, France*

²*Université Montpellier 2, CNRS, LMGC, Rue de St. Priest, 34095, Montpellier, France*

³*Laboratoire EM2C, CNRS, Ecole Centrale Supelec, Université Paris-Saclay, France*

⁴*Université de Lille 1, CNRS, IEMN, Avenue Poincaré, 59652, Villeneuve d'Ascq, France*

⁵*LIMMS/CNRS-IIS (UMI2820), Institute of Industrial Science, University of Tokyo, 4-6-1 Komaba, Meguro-ku, Tokyo 153-8505, Japan*

* ahmed.alwakil@fresnel.fr

Abstract: Thermal radiation is a universal property for all objects with temperatures above 0K. Every object with a specific shape and emissivity has its own thermal radiation signature; such signature allows the object to be detected and recognized which can be an undesirable situation. In this paper, we apply transformation optics theory to a thermal radiation problem to develop an electromagnetic illusion by controlling the thermal radiation signature of a given object. Starting from the fluctuation dissipation theorem where thermally fluctuating sources are related to the radiative losses, we demonstrate that it is possible for objects residing in two spaces, virtual and physical, to have the same thermal radiation signature if the complex permittivities and permeabilities satisfy the standard space transformations. We emphasize the invariance of the fluctuation electrodynamics physics under transformation, and show how this result allows the mimicking in thermal radiation. We illustrate the concept using the illusion paradigm in the two-dimensional space and a numerical calculation validates all predictions. Finally, we discuss limitations and extensions of the proposed technique.

References and links

1. J. B. Pendry, D. Schurig, and D. R. Smith, "Controlling Electromagnetic Fields," *Science* **312**(5781), 1780–1782 (2006).
2. D. Schurig, J. B. Pendry, and D. R. Smith, "Calculation of material properties and ray tracing in transformation media," *Opt. Express* **14**(21), 9794–9804 (2006).
3. U. Leonhardt, "Optical Conformal Mapping," *Science* **312**(5781), 1777–1780 (2006).
4. V. M. Shalaev, "Physics. Transforming Light," *Science* **322**(5900), 384–386 (2008).
5. U. Leonhardt and T. G. Philbin, "Transformation Optics and the Geometry of Light," *Prog. Opt.* **53**, 69–152 (2009).
6. R. Fleury and A. Alu, "Cloaking and Invisibility: a Review (Invited Review)," *Prog. Electromagnetics Res.* **147**, 171–202 (2014).
7. Y. Lai, J. Ng, H. Chen, D. Han, J. Xiao, Z.-Q. Zhang, and C. T. Chan, "Illusion Optics: The Optical Transformation of an Object into Another Object," *Phys. Rev. Lett.* **102**(25), 253902 (2009).
8. T. Yang, H. Chen, X. Luo, and H. Ma, "Superscatterer: Enhancement of scattering with complementary media," *Opt. Express* **16**(22), 18545–18550 (2008).
9. H. Chen, X. Luo, H. Ma, and C. T. Chan, "The Anti-Cloak," *Opt. Express* **16**(19), 14603–14608 (2008).
10. G. Castaldi, I. Gallina, V. Galdi, A. Alù, and N. Engheta, "Cloak/anti-cloak interactions," *Opt. Express* **17**(5), 3101–3114 (2009).
11. Y. Lai, H. Chen, Z.-Q. Zhang, and C. T. Chan, "Complementary Media Invisibility Cloak that Cloaks Objects at a Distance Outside the Cloaking Shell," *Phys. Rev. Lett.* **102**(9), 093901 (2009).
12. X. Zang and C. Jiang, "Overlapped optics, illusion optics, and an external cloak based on shifting media," *JOSA B* **28**(8), 1994–2000 (2011).

13. S. Guenneau, C. Amra, and D. Veynante, "Transformation thermodynamics: cloaking and concentrating heat flux," *Opt. Express* **20**(7), 8207–8218 (2012).
14. M. Raza, Y. Liu, E. H. Lee, and Y. Ma, "Transformation thermodynamics and heat cloaking: a review," *J. Opt.* **18**(4), 044002 (2016).
15. T. Han and C.-W. Qiu, "Transformation Laplacian metamaterials: recent advances in manipulating thermal and dc fields," *J. Opt.* **18**(4), 044003 (2016).
16. J. R. Howell, M. P. Menguc, and R. Siegel, *Thermal Radiation Heat Transfer, 5th Edition* (CRC, 2010).
17. M. F. Modest, *Radiative Heat Transfer* (Academic, 2003).
18. G. Gaussorgues and S. Chomet, *Infrared Thermography* (Springer Science & Business Media, 1993).
19. P. Xavier, Maldague, *Nondestructive Evaluation of Materials by Infrared* (Springer, 2017).
20. D. A. B. Miller, "On perfect cloaking," *Opt. Express* **14**(25), 12457–12466 (2006).
21. F. G. Vasquez, G. W. Milton, and D. Onofrei, "Active Exterior Cloaking for the 2D Laplace and Helmholtz Equations," *Phys. Rev. Lett.* **103**(7), 073901 (2009).
22. H. H. Zheng, J. J. Xiao, Y. Lai, and C. T. Chan, "Exterior optical cloaking and illusions by using active sources: A boundary element perspective," *Phys. Rev. B* **81**(19), 195116 (2010).
23. M. Selvanayagam and G. V. Eleftheriades, "An Active Electromagnetic Cloak Using the Equivalence Principle," *IEEE Antennas Wirel. Propag. Lett.* **11**, 1226–1229 (2012).
24. D. L. Sounas, R. Fleury, and A. Alù, "Unidirectional Cloaking Based on Metasurfaces with Balanced Loss and Gain," *Phys. Rev. Appl.* **4**(1), 014005 (2015).
25. S. M. Burkinshaw, G. Hallas, and A. D. Towns, "Infrared camouflage," *Rev. Prog. Color. Relat. Top.* **26**(1), 47–53 (1996).
26. S. Wijewardane and D. Y. Goswami, "A review on surface control of thermal radiation by paints and coatings for new energy applications," *Renew. Sustain. Energy Rev.* **16**(4), 1863–1873 (2012).
27. P. Bamfield and M. G. Hutchings, *Chromic Phenomena: Technological Applications of Colour Chemistry* (Royal Society of Chemistry, 2010).
28. K. K. Gupta, A. Nishkam, and N. Kasturiya, "Camouflage in the Non-Visible Region," *J. Ind. Text.* **31**(1), 27–42 (2001).
29. M. A. Kats, R. Blanchard, S. Zhang, P. Genevet, C. Ko, S. Ramanathan, and F. Capasso, "Vanadium Dioxide as a Natural Disordered Metamaterial: Perfect Thermal Emission and Large Broadband Negative Differential Thermal Emittance," *Phys. Rev. X* **3**(4), 041004 (2013).
30. R. F. Reynolds and M. J. Kinsella, "Thermal and visual camouflage system," U.S. patent US6338292 B1 (January 15, 2002).
31. S. M. Rytov, *Theory of Electric Fluctuations and Thermal Radiation*. (Electronics Research Directorate, Air Force Cambridge Research Center, Air Research and Development Command, U.S. Air Force., 1959).
32. C. Henkel, "Nanoscale Thermal Transfer – An Invitation to Fluctuation Electrodynamics," *Z. Für Naturforschung A* **72**, 99–108 (2016).
33. Y. Zheng, "Review of fluctuational electrodynamics and its applications to radiative momentum, energy and entropy transport," ArXiv14105741 Cond-Mat (2014).
34. H. B. Callen and T. A. Welton, "Irreversibility and Generalized Noise," *Phys. Rev.* **83**(1), 34–40 (1951).
35. J. Weber, "Fluctuation Dissipation Theorem," *Phys. Rev.* **101**(6), 1620–1626 (1956).
36. R. Kubo, "The fluctuation-dissipation theorem," *Rep. Prog. Phys.* **29**(1), 255–284 (1966).
37. D. Polder and M. Van Hove, "Theory of Radiative Heat Transfer between Closely Spaced Bodies," *Phys. Rev. B* **4**(10), 3303–3314 (1971).
38. J. B. Pendry, "Radiative exchange of heat between nanostructures," *J. Phys. Condens. Matter* **11**(35), 6621–6633 (1999).
39. N. Kundtz, D. A. Roberts, J. Allen, S. Cummer, and D. R. Smith, "Optical source transformations," *Opt. Express* **16**(26), 21215–21222 (2008).
40. S. A. Cummer, N. Kundtz, and B.-I. Popa, "Electromagnetic surface and line sources under coordinate transformations," *Phys. Rev. A* **80**(3), 033820 (2009).
41. P. H. Tichit, J. Yi, S. N. Burokur, and A. de Lustrac, "Application of transformation electromagnetics concept to delocalize emissions," in *2015 9th European Conference on Antennas and Propagation (EuCAP)* (2015), 1–4.
42. J. Zhang, M. Wubs, P. Ginzburg, G. Wurtz, and A. V. Zayats, "Transformation quantum optics: designing spontaneous emission using coordinate transformations," *J. Opt.* **18**(4), 044029 (2016).
43. M. Morshed Behbahani, E. Amooghorban, and A. Mahdifar, "Spontaneous emission and the operation of invisibility cloaks," *Phys. Rev. A* **94**(1), 013854 (2016).
44. R. Zhao, Y. Luo, A. I. Fernández-Domínguez, and J. B. Pendry, "Description of van der Waals Interactions Using Transformation Optics," *Phys. Rev. Lett.* **111**(3), 033602 (2013).
45. R. Zhao, Y. Luo, and J. B. Pendry, "Transformation optics applied to van der Waals interactions," *Sci. Bull.* **61**(1), 59–67 (2016).
46. B.-I. Popa and S. A. Cummer, "Complex coordinates in transformation optics," *Phys. Rev. A* **84**(6), 063837 (2011).
47. W. Eckhardt, "First and second fluctuation-dissipation-theorem in electromagnetic fluctuation theory," *Opt. Commun.* **41**(5), 305–309 (1982).
48. J.-J. Greffet, P. Bouchon, G. Brucoli, E. Sakat, and F. Marquier, "Generalized Kirchhoff law," ArXiv160100312 Phys. (2016).

49. J. G. V. Bladel, *Electromagnetic Fields* (John Wiley & Sons, 2007).
 50. J. Guan, W. Li, W. Wang, and Z. Fu, "General boundary mapping method and its application in designing an arbitrarily shaped perfect electric conductor reshapener," *Opt. Express* **19**(20), 19740–19751 (2011).
 51. C. Li and F. Li, "Two-dimensional electromagnetic cloaks with arbitrary geometries," *Opt. Express* **16**(17), 13414–13420 (2008).
 52. G. Dupont, S. Guenneau, S. Enoch, G. Demesy, A. Nicolet, F. Zolla, and A. Diatta, "Revolution analysis of three-dimensional arbitrary cloaks," *Opt. Express* **17**(25), 22603–22608 (2009).
 53. W. X. Jiang, J. Y. Chin, Z. Li, Q. Cheng, R. Liu, and T. J. Cui, "Analytical design of conformally invisible cloaks for arbitrarily shaped objects," *Phys. Rev. E Stat. Nonlin. Soft Matter Phys.* **77**(6 Pt 2), 066607 (2008).
 54. A. Nicolet, F. Zolla, and S. Guenneau, "Electromagnetic analysis of cylindrical cloaks of an arbitrary cross section," *Opt. Lett.* **33**(14), 1584–1586 (2008).
 55. S. Guenneau, D. Petiteau, M. Zerrad, and C. Amra, "Bicephalous transformed media: concentrator versus rotator and cloak versus superscatterer," *Opt. Express* **22**(19), 23614–23619 (2014).
 56. C. Garcia-Meca and C. Barceló, "Nontensorial Transformation Optics," *Phys. Rev. Appl.* **5**(6), 064008 (2016).
 57. K. Chen and S. Fan, "Nonequilibrium Casimir Force with a Nonzero Chemical Potential for Photons," *Phys. Rev. Lett.* **117**(26), 267401 (2016).
 58. K. Chen, P. Santhanam, S. Sandhu, L. Zhu, and S. Fan, "Heat-flux control and solid-state cooling by regulating chemical potential of photons in near-field electromagnetic heat transfer," *Phys. Rev. B* **91**(13), 134301 (2015).
 59. R. Graham and H. Haken, "Quantum theory of light propagation in a fluctuating laser-active medium," *Z. Für Phys. Hadrons Nucl.* **213**(5), 420–450 (1968).
 60. C. Khandekar, W. Jin, O. D. Miller, A. Pick, and A. W. Rodriguez, "Giant frequency-selective near-field energy transfer in active/passive structures," *Phys. Rev. B* **94**(11), 115402 (2016).
 61. A. Alwakil, M. Zerrad, M. Bellieud, and C. Amra, "Inverse heat mimicking of given objects," *Sci. Rep.* **7**, 43288 (2017).
 62. K. Joulain, J.-P. Mulet, F. Marquier, R. Carminati, and J.-J. Greffet, "Surface electromagnetic waves thermally excited: Radiative heat transfer, coherence properties and Casimir forces revisited in the near field," *Surf. Sci. Rep.* **57**(3-4), 59–112 (2005).
-

1. Introduction

Transformation optics (TO) [1–5] has been an active domain of research with key applications such as electromagnetic cloaking, camouflage and illusion [6]. Most often passive objects are coated with a TO-designed cloak to generate a zero scattering cross-section in case of perfect cloaking, or a scattering cross-section similar to that of another object in case of optical illusion [7–12]. The same concept was extended to heat transfer physics through thermal conduction in solids [13–15]. Here, we extend TO to thermal radiation (TR) and the technique is applied to control TR signatures emitted from arbitrary objects in order, for instance, to deceive a detector thanks to a countermeasure effect changing its shape.

TR is an incoherent electromagnetic radiation from objects at temperature above 0K [16,17]. All objects thermally radiate and their TR signature (i.e., spectral and spatial distribution of the emission) depends on their shape and constitutive parameters. Typically, passive infrared surveillance is such that a thermally radiating object is detected by devices sensitive to wavelengths around the maximal emission. TR detection is generally operated in two infrared ranges (3–5 μm) and (8–14 μm) [18,19]. Within this framework, camouflage or cloak techniques are either active or passive. In the first (active) situation, the emitter is surrounded by controllable sources that emit in the same frequency range indicating different shapes and temperature [20–24]; in the second (passive) one, the TR signatures of the cloaked objects are cancelled so as to minimize the contrast with the environment (typically air). This can be achieved by covering the emitter with low-emissivity paints [25–28] or phase transition thermal layers [29] fabricated to keep the thermal emission close to that of the background, thanks to the control of their infrared reflectance. However such techniques have to face the challenge of time temperature increase due to such isolation [30], hence limiting their usage to relatively short time. Notice also that the environment may vary with time (case of moving objects), which is another difficulty.

There are at least two theoretical tools to examine TR at the macroscopic level. With the first one TR is visualized as geometric rays which carry the radiated energy and the resulting pattern is governed by the Radiative Transfer Equation (RTE) [16]. This equation relies on

mere conservation of radiative intensity along lines of sight between thermal emitter and observer. RTE provides a satisfactory model for TR in most far field applications. However, most often it ignores the phase and vector properties of TR, for which reason it is not optimally suitable to be integrated with TO theory. The second tool is Fluctuation electrodynamics (FE) introduced by Rytov [31], where TR is treated as an electromagnetic radiation originating from randomly thermally fluctuating electric and magnetic volumetric current sources [32,33]. These sources are governed by stochastic processes and their statistical properties are determined by the Fluctuation dissipation theorem (FDT) which relates the losses of a linear system to the fluctuations of its internal thermal energy [34–36]. FE is typically used in cases where RTE fails, for instance, in describing near field thermal radiation [37,38].

Transformation optics describe the equivalence between space deformation and modification of materials physical parameters. In other words, Maxwell equations and the associated electromagnetic field cannot “see” the difference between the curvature of the space by on one hand and the inhomogeneity and anisotropy of the medium on the other hand [5]. Such invariance of Maxwell equations allows for the equivalence between different systems as long as the transformed material parameters between the two spaces satisfy the adequate transformations. If electromagnetic sources are included, source transformation [39–41] must also be employed. Typically, transformations are performed between different spaces including different current densities or antennas, and modify the antenna surrounding in order to mimic the same radiation pattern outside a predefined cloak frontier.

In this paper, we first show that FE is invariant under transformations depicted by TO, in the sense that the same fluctuation dissipation theorem is recovered in the physical space after transformation of both the physical parameters and the thermal sources. For that the thermal current sources are first transformed in the same manner as coherent sources according to source transformation, and these transformed sources are then compared to those which are proportional to dissipative losses in the physical space. Hence both ways of transforming the thermal currents are consistent and only constrained by the validity of FDT in both spaces. In order to keep the model relevant to the ongoing literature of near field thermal radiation [32], we illustrate our theoretical demonstration by considering the two-dimensional (2D) space where the electromagnetic radiation is the combination of Transverse Electric (TE) and Transverse Magnetic (TM) polarizations. To the authors’ knowledge, no other work has yet addressed the application of the TO theory to FE. Similar theoretical studies were implemented using TO in the realm of Quantum optics [42,43] in order to control spontaneous emission from quantum emitter, and others have treated van der Waals forces [44,45].

2. Transformation optics and fluctuation electrodynamics

TO theory states that in order to keep Maxwell’s equations invariant under a transformation between a departure (pre-transformation) space with the coordinate set $\{x^m\}$ and another arrival (post-transformation) space with the coordinate set $\{x^{m'}\}$, the material’s parameters must comply with the following transformation [5]:

$$\varepsilon^{m'n'} = \frac{1}{|\underline{A}|} A_m^{m'} A_n^{n'} \varepsilon^{mn} \text{ and } \mu^{m'n'} = \frac{1}{|\underline{A}|} A_m^{m'} A_n^{n'} \mu^{mn}, \quad (1)$$

where $A_m^{m'} = \frac{\partial x^{m'}}{\partial x^m}$ and $|\underline{A}|$ are the elements and the determinant of the Jacobian matrix \underline{A} , ε and μ are the relative permittivity and permeability tensors respectively. Note that m', n', m and n are indices of the space coordinates, respectively used for $\{x', y', z'\}$ and $\{x, y, z\}$. Here, we assume that the transformation is real (i.e.: associates real-valued coordinate systems), in contrast to complex valued transformations [46]. The media in both departure and arrival spaces are lossy so that their permittivity or permeability are complex valued functions. We

exclude the cases of bi-anisotropic and optical active media. We consider a $e^{i\omega t}$ time harmonic dependence, where ω is the angular frequency and t is referring to time. It is supposed that the imaginary parts of permittivity and permeability tensors $\text{Im}\{\epsilon^{mn}\}$ and $\text{Im}\{\mu^{mn}\}$ are positive tensors, which is characteristic of a passive medium (no gain). If the departure space contains nonzero electric (J) and magnetic (K) volumetric current sources, then these current sources are also transformed to the arrival space as follows [39]:

$$J^{m'} = \frac{1}{|\underline{A}|} A_m^{m'} J^m \text{ and } K^{m'} = \frac{1}{|\underline{A}|} A_m^{m'} K^m. \quad (2)$$

FDT theory states that for any dissipative linear system with local thermodynamical temperature T , the spectral density of the generalized force of the system fluctuates in such a way to be proportional to the dissipative part of the transfer function of the system [34]. Here we consider the FDT of second kind [47] where TR is the electromagnetic response to the stochastic current sources. The spectral correlation of the volumetric electric J^m and magnetic currents K^m embedded in the object, with relative complex permittivity tensor $\epsilon^{mn}(x, \omega)$ and relative complex permeability tensor $\mu^{mn}(x, \omega)$ is quantified as follows [48]:

$$\langle J^m(x_1; \omega_1) J^{n*}(x_2; \omega_2) \rangle = \frac{\omega \epsilon_0}{\pi} \theta(\omega, T) \text{Im}\{\epsilon^{mn}(x_1; \omega_1)\} \delta(x_1 - x_2) \delta(\omega_1 - \omega_2). \quad (3)$$

$$\langle K^m(x_1; \omega_1) K^{n*}(x_2; \omega_2) \rangle = \frac{\omega \mu_0}{\pi} \theta(\omega, T) \text{Im}\{\mu^{mn}(x_1; \omega_1)\} \delta(x_1 - x_2) \delta(\omega_1 - \omega_2). \quad (4)$$

where $\langle \rangle$ represents an ensemble average, $\theta(\omega, T) = h\omega \left(e^{h\omega/k_B T} - 1 \right)^{-1}$ corresponds to the mean energy of a single quantum oscillator with angular frequency ω , ignoring vacuum fluctuations. x_1 and x_2 are two different position vectors in the thermal emitter. δ indicates Dirac functions, k_B is Boltzmann's constant, ϵ_0 and μ_0 are the permittivity and permeability of the free space respectively. The star (*) indicates the complex conjugation operator. Once the thermally fluctuating sources have been quantified, the radiated field can be computed by solving Maxwell's equations, or equivalently knowing the Green's function for both electric and magnetic fields.

3. Transformational fluctuation electrodynamics

In this section, we apply the TO theory to the FE problem. Starting with a lossy object characterized by ϵ^{mn} and μ^{mn} residing in the departure space, the correlation of fluctuating electric and magnetic currents is provided according to (3) and (4). Hence these correlations are proportional of the imaginary permittivity and permeability of the departure space. Now transforming from the departure space into another arrival space with transformation $A_m^{m'}$, the arrival object's parameters $\epsilon^{m'n'}$ and $\mu^{m'n'}$ are transformed according to (1). Since electric and magnetic currents are transformed according to (2), then, the transformation of the spectral correlation of the fluctuational electric current follows:

$$\langle J^{m'}(x'_1; \omega_1) J^{n*}(x'_2; \omega_2) \rangle = \frac{1}{|\underline{A}|^2} A_m^{m'} A_n^{n'} \langle J^m(x_1; \omega_1) J^{n*}(x_2; \omega_2) \rangle. \quad (5)$$

substituting the right-hand side correlation with (3), then

$$\langle J^{m'}(x'_1; \omega_1) J^{n*}(x'_2; \omega_2) \rangle = \frac{1}{|\underline{A}|^2} A_m^{m'} A_n^{n'} \frac{\omega \mathcal{E}_0}{\pi} \theta(\omega, T) \text{Im}\{\varepsilon^{mn}(x_1; \omega_1)\} \delta(x_1 - x_2) \delta(\omega_1 - \omega_2). \quad (6)$$

due to its scaling property [49], the delta function is transformed as follows:

$$\delta(x'_1 - x'_2) = \frac{1}{|\underline{A}|} \delta(x_1 - x_2). \quad (7)$$

substituting (1) and (7) in (6) yields:

$$\langle J^{m'}(x'_1; \omega_1) J^{n*}(x'_2; \omega_2) \rangle = \frac{\omega \mathcal{E}_0}{\pi} \theta(\omega, T) \text{Im}\{\varepsilon^{m'n'}(x'_1; \omega_1)\} \delta(x'_1 - x'_2) \delta(\omega_1 - \omega_2). \quad (8)$$

Similarly,

$$\begin{aligned} \langle K^{m'}(x'_1; \omega_1) K^{n*}(x'_2; \omega_2) \rangle &= \frac{1}{|\underline{A}|^2} A_m^{m'} A_n^{n'} \langle K^m(x_1; \omega_1) K^{n*}(x_2; \omega_2) \rangle \\ &= \frac{\omega \mu_0}{\pi} \theta(\omega, T) \text{Im}\{\mu^{m'n'}(x'_1; \omega_1)\} \delta(x'_1 - x'_2) \delta(\omega_1 - \omega_2). \end{aligned} \quad (9)$$

These last relations show that after space transformation, the current correlations in the arrival space are again proportional to the imaginary parts of permittivity and permeability of the arrival space. Hence, from Eqs. (3), (8) and (4), (9), FDT has the same form after transformation, that is, the source correlations resulting from the FDT theorem in the arrival space is identical to the transformation of the source correlations resulting from the FDT theorem in the departure space. We therefore conclude that FE is invariant under TO transformations. We also notice that such invariance requires a real-valued transformation.

These last remarks introduce the proposed camouflage technique, which consists in engineering the losses of a given object and its surrounding to control its emitted TR signature. Notice usually that both media (materials) and sources (currents) must be engineered or micro-structured independently to satisfy the transformation optics and the mimicking effect; here the FE invariance proves that there is no need to engineer the source in the arrival space, which is the key property which allows the TR mimicking.

In the next section, we illustrate the developed theory using a 2D case where the system is invariant along the out of plane axis. Two-dimensional electromagnetic scattering cloaking/camouflage was studied previously [50–55]. In this paper, we extend this analysis to its TR counterpart.

4. Two dimensional TE/TM camouflages

In this section, we show how to transform a TR problem between two spaces to produce a TR illusion. We consider an illustrative numerical example of transformation between 2D spaces. As shown in Fig. 1, the departure space includes a thermally radiating circular shaped object (with radius r_0) surrounded by a circular coating (with radius r_{ex}). It is desired that when thermally radiating, these cylinders mimic the TR signature of a horizontal elliptical shaped object (with the outer boundary defined by the radial distance $\rho(x, y)$) for its TE polarization, and simultaneously mimic the TR signature of a vertical elliptical shaped object (with the outer boundary defined by the radial distance $\eta(x, y)$) for its TM polarization. The objects in all spaces are assumed to be embedded in a non-absorbing background medium in such a way that the areas surrounding the objects, including the coating, do not contribute to TR (at least the coating can be engineered in such a way that its thermal radiation is appreciably less than the target in the frequency band). Hence the radiated field within an arbitrary line of sight will

be the superposition of the thermal radiation of the two polarizations. The departure space is chosen to be the physical space for both polarizations, while the virtual space for each polarization is chosen to be the arrival space of the corresponding assigned transformations. If the detector is polarization insensitive, the observer will detect both the vertical and horizontal elliptical shaped objects simultaneously giving the illusion - for the observer- that the two objects coincide.

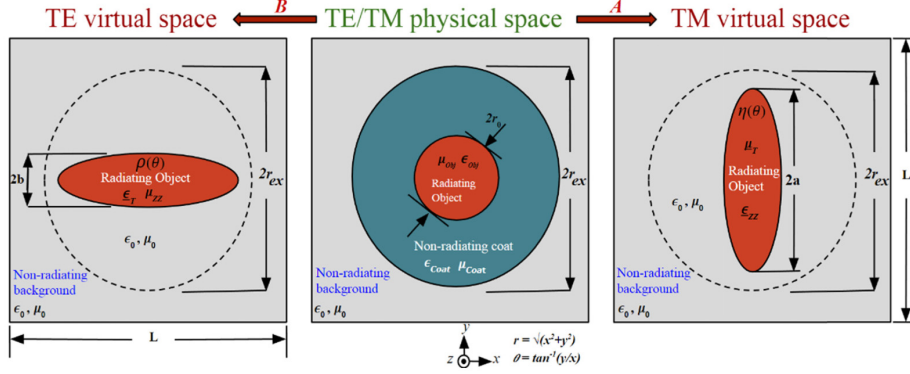


Fig. 1. schematic of the TR illusion example discussed in section 4. The middle figure is for the TE/TM physical space (departure space) with a homogenous anisotropic lossy circular object with radius r_0 [$\epsilon_{obj}^{mn} = \delta^{mn} (3 + i0.02)$ and $\mu_{obj}^{mn} = \delta^{mn} (1 + i0.02\delta^{mz})$] coated with an inhomogeneous anisotropic circular coat with radius r_{ex} . The left figure is for the TE virtual space with inhomogeneous anisotropic horizontal elliptical shaped object with semi-axes a and b embedded in a homogenous medium. The right figure is similar but for a vertical ellipse and for TM polarization. The region outside r_{ex} is unity transformed for both polarizations. The areas of all spaces between the dotted external cylinder and the virtual or physical objects, are lossless and do not contribute to the thermal radiation. For numerical calculations, L was set to be 11.1λ with matched boundary conditions at the square frames.

Appendix (A) summarizes the differential equations for both TM and TE polarizations in both spaces and gives the transformation of different fields between the two spaces. As shown in the appendix (A), TM and TE problems are independent, which allows to mimic one object (horizontal or vertical ellipse) per polarization. It is therefore possible to have two independent transformations \underline{A} and \underline{B} for TM and TE polarizations respectively. We provide here an illustration for the TM case but the quantities for the TE case can be retrieved by considering the duality between both polarizations and replacing $\eta(\theta)$ by $\rho(\theta)$. Considering the TM case, the simplest form of the coordinate transformation A can be written as follows:

$$r' = \frac{\eta(\theta)}{r_0} r \text{ and } \theta' = \theta \text{ object transformation } (0 < r < r_0). \quad (10)$$

Notice here that (x, y) and (r, θ) are the Cartesian and polar coordinates of the departure space, while (x', y') and (r', θ') are the Cartesian and polar coordinates of the arrival space. Now, to design the coat parameters, a transformation is done from the surrounding medium in the virtual space, ensuring continuity at the inner and outer boundaries of the coat ($\eta < r < r_{ex}$) as follows:

$$r = \begin{cases} \frac{r_{ex} - r_0}{r_{ex} - \eta} (r' - r_{ex}) + r_{ex} \rightarrow (\eta < r < r_{ex}) \text{ and } (\eta < r' < r_{ex}). \\ r' \rightarrow (r > r_{ex}) \text{ and } (r' > r_{ex}). \end{cases} \quad (11)$$

$$\theta' = \theta.$$

Relations (10-11) are the basis for the TO transformation of the physical parameters. As a result, the inhomogeneous regions are the two ellipses of the virtual spaces and the cylinder cloak of the physical space, while the cylinder itself and the cloaks of both virtual spaces are homogeneous. In general, all media are anisotropic in regions $r < r_{ex}$ but, for simplicity, we assume that the circular object residing inside the TE/TM physical space of Fig. 1 (middle figure) has a diagonal homogenous permittivity and permeability. Consequently, the electric current densities that are embedded in this object and polarized in orthogonal directions are uncorrelated i.e.: $\langle J^x J^{y*} \rangle = 0$. Furthermore, as shown in appendix (A) and following Eq. (2), the transverse electric current densities of the TM case are transformed as follows:

$$J^{x'} = \frac{1}{\sqrt{|A|}} A_x^{x'} J^x + \frac{1}{\sqrt{|A|}} A_y^{x'} J^y \quad \text{and} \quad J^{y'} = \frac{1}{\sqrt{|A|}} A_x^{y'} J^x + \frac{1}{\sqrt{|A|}} A_y^{y'} J^y. \quad (12)$$

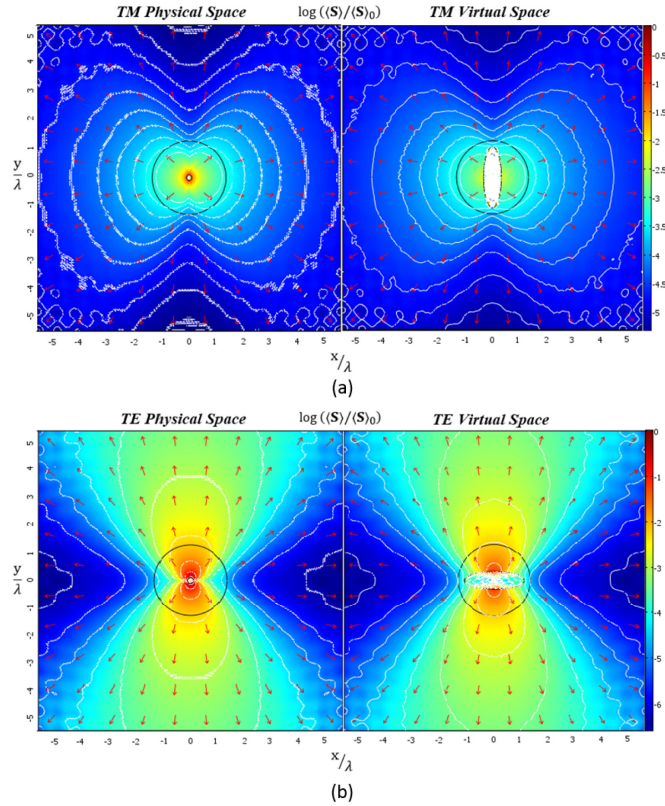


Fig. 2. Numerical calculation of normalized time averaged radiated poynting vector (log scale) at the virtual and physical spaces of TE and TM as depicted in Fig. 1, (a) TM physical (left) and virtual (right) (b) TE physical (left) and virtual (right). Colored surfaces, red arrows and white contours indicate the modulus (log scale), direction and isocontours of the poynting vector respectively. The left figures consider the circular radiating cylinder given in the middle part of Fig. 2. These left figures give the TR pattern of the cylinder coated to mimic the TR patterns of vertical (Fig. 2(a)) and horizontal (Fig. 2(b)) ellipses for TE and TM polarizations (see text). The right figures consider the vertical and horizontal coated ellipses of Fig. 1. These right figures give the TR pattern of the ellipses for each polarization and these patterns must be compared to those of the left figures. Normalization constants are: for TM, $\langle S \rangle_0 = 5.7 \times 10^{-33}$ W/m², while for TE, $\langle S \rangle_0 = 10^{-28}$ W/m². We notice that the emitted power has the same distribution outside the transformation regions for both polarizations at the physical and virtual spaces. Slight differences between both spaces are attributed to numerical error of discretization.

Similarly, the z-component of the magnetic current is transformed as:

$$K'_z = \frac{K_z}{|A|}. \quad (13)$$

We calculated the harmonic time averaged Poynting vector of the emitted field and COMSOL Multiphysics was used for the numerical implementation. In Appendix (B) the analytical expressions of this radiated pointing vector are derived in terms of the Green functions of the differential equation for each polarization, while appendix (C) summarizes the way the setup of the numerical calculations was held. As shown in Figs. 2(a) and 2(b), for each polarization the emitted power has the same pattern outside the cloak both in the physical and virtual spaces, which proves that the coat has allowed a successful mimicking as predicted. The imaginary part of the parameters was chosen such that the emitted radiation for both polarizations have distinct patterns. The parameters involved in the physical space object are:

$$\varepsilon_{xx} = \varepsilon_{yy} = 3 + i0.02, \varepsilon_{zz} = 3 + i0.02, \mu_{xx} = \mu_{yy} = 1 \text{ and } \mu_{zz} = 1 + i0.02 \quad (14)$$

hence the permittivity is isotropic but the permeability is not. Notice that ε_{xx} , ε_{yy} and μ_{zz} are involved in the TE problem, while μ_{xx} , μ_{yy} and ε_{zz} are involved in the TM problem. The radial distance for the horizontal and vertical ellipses are respectively:

$$\eta(\theta) = \left[\left(\frac{\cos(\theta)}{b} \right)^2 + \left(\frac{\sin(\theta)}{a} \right)^2 \right]^{-1/2} \text{ and } \rho(\theta) = \eta \left(\theta \pm \frac{\pi}{2} \right). \quad (15)$$

Slight differences can be seen and must be attributed to numerical error of discretization. The external coating radius is $r_{\text{ex}} = (4/3) \lambda$, the physical space object radius is $r_0 = (1/9) \lambda$, while the semi-axis of the virtual space objects is $a = (10/9) \lambda$ and $b = (1/3) \lambda$. Calculation is performed for the near field. Such a calculation can be scaled to any arbitrary wavelength, considering material's dispersion. The choice of the dimensions (small size of the radiating objects) results from our limited computational power, but similar results would be obtained for micrometer wavelengths and meter objects. To conclude this section, since the Poynting vector of the thermal radiation in the physical and virtual spaces are identical for both polarizations outside the transformation region, then the developed theory is confirmed within our hypothesis framework.

5. Conclusion and perspectives

We have introduced and validated a Transformation Optics (TO) based technique to manipulate the Thermal Radiation (TR) signature for camouflage or illusion purposes. We showed that Fluctuation Electrodynamics (FE) is invariant under TO, so that by engineering the parameters of the materials in the physical space, one can get the same TR signature than another one emitted in the virtual space. The concept was illustrated by a numerical example employing a 2D space transformation. For this example, we used a double mimicking procedure (one per polarization) which is the extension of a previous double cloaking procedure [55].

Although the proposed tool seems promising, limitations must be emphasized. For instance, realizing TO based designs remains a substantial challenge since the resultant parameters after transformation are nonhomogeneous tensorial parameters. One way to simplify the design is to incorporate non-tensorial TO [56]. Otherwise homogenization techniques must be addressed, but the dispersion laws of the physical parameters should also be controlled for the TR illusion to work in a wide spectral range.

Furthermore, according to Eqs. (3-4) and (8-9), another limitation lies on the fact that the objects have the same temperature in both virtual and physical spaces; such difficulty could

conceptually be overcome by manipulating the chemical potential of photons with an electric potential applied on a semiconductor medium to shift its effective temperature [57,58].

The transformations that we used were single valued so that every point in the virtual space was mapped to a unique image in the physical space. Notice that multi-valued transformations were typically used in the context of overlapping illusion optics [12] and anti-cloaks [9,10] where the image has a larger scattering cross section than that of the virtual space; they were also used for shifting transformations where the image is “seen” at different locations [11], [41] and size [8] than those of the original object. We restricted the frame to lossy media with positive imaginary parts for permittivity and permeability, and the temperature was assumed positive. To achieve multivalued transformation, such assumptions must be relaxed. For example, a negative real permittivity was employed to produce anti-cloaks [9]. To implement TR analog of the anti-cloak, a negative imaginary permittivity (permeability) media (gain media) is required. However, the self-correlation of current densities must always be a positive quantity, for which reason a modified version of FDT must be used [59,60]. It was mentioned in [60] that a population inverted two level system gain media exhibits a negative effective temperature such that Planck distribution is negative. Negative Planck distribution can be also achieved by controlling the photonic chemical potential [57,58]. Finally, Thermal radiation illusion of objects with graded temperature is possible by simultaneous transformation of thermal conductivities [61] and electromagnetic constitutive parameters.

Appendix A: two dimensional TE/TM formulations

Starting with Maxwell’s equations and assuming invariance along z-axis, the TR problem is decomposed into two independent problems that are the TM polarization (Magnetic field is polarized in the z-direction) and the TE polarization (Electric field is polarized in the z-direction). Here we adopt a notation similar to that used in [55], where TM and TE polarizations were transformed using independent transformations A and B respectively. Let us rewrite all the tensorial quantities in terms of transverse (x and y) components and z-components as follows:

$$\underline{\underline{\epsilon}}^{mn} = \begin{pmatrix} \underline{\underline{\epsilon}}_T & 0 \\ 0 & \epsilon_{zz} \end{pmatrix}, \underline{\underline{\mu}}^{mn} = \begin{pmatrix} \underline{\underline{\mu}}_T & 0 \\ 0 & \mu_{zz} \end{pmatrix}, J^m = \begin{pmatrix} \underline{J}_T \\ J_z \end{pmatrix}, K^m = \begin{pmatrix} \underline{K}_T \\ K_z \end{pmatrix}, E^m = \begin{pmatrix} \underline{E}_T \\ E_z \end{pmatrix}, H^m = \begin{pmatrix} \underline{H}_T \\ H_z \end{pmatrix}$$

$$\underline{\underline{\epsilon}}^{m'n'} = \begin{pmatrix} \underline{\underline{\epsilon}}'_T & 0 \\ 0 & \epsilon'_{zz} \end{pmatrix}, \underline{\underline{\mu}}^{m'n'} = \begin{pmatrix} \underline{\underline{\mu}}'_T & 0 \\ 0 & \mu'_{zz} \end{pmatrix}, J^{m'} = \begin{pmatrix} \underline{J}'_T \\ J'_z \end{pmatrix}, K^{m'} = \begin{pmatrix} \underline{K}'_T \\ K'_z \end{pmatrix}, E^{m'} = \begin{pmatrix} \underline{E}'_T \\ E'_z \end{pmatrix} \text{ and } H^{m'} = \begin{pmatrix} \underline{H}'_T \\ H'_z \end{pmatrix}.$$

E and H are the electric and the magnetic fields respectively. Single underlining indicates vectors while double underlining indicates matrices, subscript T indicates transverse components and $m, n = \{x, y, z\}$. Following the typical procedure of transforming Maxwell’s equations for each polarization, the differential equation for TM virtual space will be as follows:

$$\nabla \times \underline{\underline{\epsilon}}_T^{-1} \circ \nabla \times (H_z \vec{z}) - k_0^2 \mu_{zz} (H_z \vec{z}) = \nabla \times \underline{\underline{\epsilon}}_T^{-1} \circ \underline{J}_T + i\omega \epsilon_0 (K_z \vec{z}). \quad (16)$$

Notice that \circ indicates inner tensor product. The differential equation for the physical space at the same TM polarization

$$\nabla' \times \underline{\underline{\epsilon}}_T'^{-1} \circ \nabla' \times (H'_z \vec{z}) - k_0^2 \mu'_{zz} (H'_z \vec{z}) = \nabla' \times \underline{\underline{\epsilon}}_T'^{-1} \circ \underline{J}'_T + i\omega \epsilon_0 (K'_z \vec{z}). \quad (17)$$

The quantities are transformed for this TM polarization as follows:

$$\underline{\underline{\mu}}'_{zz} = \frac{\underline{\underline{\mu}}_{zz}}{\underline{\underline{A}}}, K'_z = \frac{K_z}{\underline{\underline{A}}}, \underline{\underline{\epsilon}}'_T{}^{m'n'} = \frac{1}{\underline{\underline{A}}} A_m^{m'} A_n^{n'} \underline{\underline{\epsilon}}_T^{mn}, J_T^{m'} = \frac{1}{\underline{\underline{A}}} A_m^{m'} J_T^m, \underline{\underline{E}}'_T = \underline{\underline{A}}^{-\tau} \underline{\underline{E}}_T \text{ and } H'_z = H_z. \quad (18)$$

Note that $\underline{\underline{A}}$ is the matrix form for the TM transformation and τ indicates its transpose. Similarly, for the TE virtual space we have:

$$\nabla \times \underline{\underline{\mu}}'^{-1} \circ \nabla \times (E_z \bar{z}) - k_0^2 \underline{\underline{\epsilon}}'_{zz} (E_z \bar{z}) = -\nabla \times \underline{\underline{\mu}}'^{-1} \circ \underline{\underline{K}}_T + i\omega \underline{\underline{\epsilon}}_0 (J_z \bar{z}). \quad (19)$$

and for the TE physical space:

$$\nabla' \times \underline{\underline{\mu}}'^{-1} \circ \nabla' \times (E'_z \bar{z}) - k_0^2 \underline{\underline{\epsilon}}'_{zz} (E'_z \bar{z}) = -\nabla' \times \underline{\underline{\mu}}'^{-1} \circ \underline{\underline{K}}'_T + i\omega \underline{\underline{\mu}}_0 (J'_z \bar{z}). \quad (20)$$

The quantities are transformed for this TE polarization as follows:

$$\underline{\underline{\epsilon}}'_{zz} = \frac{\underline{\underline{\epsilon}}_{zz}}{\underline{\underline{B}}}, \underline{\underline{\mu}}'_T{}^{m'n'} = \frac{1}{\underline{\underline{B}}} B_m^{m'} B_n^{n'} \underline{\underline{\mu}}_T^{mn}, K_T^{m'} = \frac{1}{\underline{\underline{B}}} B_m^{m'} K_T^m, J'_z = \frac{J_z}{\underline{\underline{B}}}, \underline{\underline{H}}'_T = \underline{\underline{B}}^{-\tau} \underline{\underline{H}}_T \text{ and } E'_z = E_z.$$

notice here that B is the matrix form of the TE transformation. It is important to mention that for both polarizations, the z-polarized fields ($E_z - H_z$) are invariant under transformation.

Appendix B: ensemble averaged poynting vectors

In this appendix we show the analytical basis for the numerical procedure given in appendix (C) and that was used to solve Eqs. (16-17) and Eqs. (19-20). We first consider the TM virtual space of Eq. (16) and start with the definition of the ensemble averaged time average Poynting vector given as:

$$\langle \underline{\underline{S}} \rangle = 4 \times \frac{1}{2} \text{Re} \left\{ \langle \underline{\underline{E}} \times \underline{\underline{H}}^* \rangle \right\}. \quad (21)$$

the scalar product of this vector with the local normal of a surface gives the elementary flux carried through this surface. The factor (4) is introduced to take into account the fact that only positive frequencies are considered in the ensemble average operator [62]. The magnetic field H_z can be calculated using the Green functions of the operator shown in Eq. (16) as follows:

$$H_z(r) = \int G_{zz}^{HH}(r, r_1) K_z(r_1) d^2 r_1 + \int G_{zx}^{HE}(r, r_2) J_T^x(r_2) d^2 r_2 + \int G_{zy}^{HE}(r, r_3) J_T^y(r_3) d^2 r_3. \quad (22)$$

similarly, for the cartesian components of the transverse electric field,

$$E_n(r) = \int G_{nz}^{EH}(r, r_4) K_z(r_4) d^2 r_4 + \int G_{nx}^{EE}(r, r_5) J_T^x(r_5) d^2 r_5 + \int G_{ny}^{EE}(r, r_6) J_T^y(r_6) d^2 r_6. \quad (23)$$

where G_{zz}^{HH} , G_{zx}^{HE} and G_{zy}^{HE} are the magnetic field Green functions of Eq. (16) due to the out of plane magnetic current density K_z and the transverse components of the electric current density J_T^x and J_T^y respectively. In a similar manner G_{nz}^{EH} , G_{nx}^{EE} and G_{ny}^{EE} are the transverse electric field components Green functions due to the latter current sources respectively, with $n = \{x, y\}$. r is the position vector of the observation point and $\{r_1, \dots, r_6\}$ are position vectors inside the thermal emitter volume. Substituting (22-23) in Eq. (21), the ensemble averaged Poynting vector will be as follows:

$$\langle \underline{\underline{S}}^{TM} \rangle = 2\bar{x} \text{Re} \left\{ \langle E_y H_z^* \rangle \right\} - 2\bar{y} \text{Re} \left\{ \langle E_x H_z^* \rangle \right\} = \bar{x} \langle S_x^{TM} \rangle + \bar{y} \langle S_y^{TM} \rangle. \quad (24)$$

substituting again with Eqs. (3) and (4) yields,

$$\begin{aligned} \langle E_y H_z^* \rangle &= \frac{\omega \mu_0}{\pi} \theta(\omega, T) \int d^2 r_1 G_{yz}^{EH}(\underline{r}, \underline{r}_1) \text{Im}\{\mu_{zz}(\underline{r}_1)\} G_{zz}^{HH*}(\underline{r}, \underline{r}_1) \\ &+ \frac{\omega \mathcal{E}_0}{\pi} \theta(\omega, T) s \int d^2 r_2 \sum_{n=x,y} \sum_{m=x,y} G_{yn}^{EE}(\underline{r}, \underline{r}_2) \text{Im}\{\varepsilon^{mn}(\underline{r}_2)\} G_{zm}^{HE*}(\underline{r}, \underline{r}_2). \end{aligned} \quad (25)$$

notice here that we used the property $\langle J_T^m K^{n*} \rangle = 0$ since the medium is non-chiral. Similarly, for the y-component,

$$\begin{aligned} \langle E_x H_z^* \rangle &= \frac{\omega \mu_0}{\pi} \theta(\omega, T) \int d^2 r_1 G_{xz}^{EH}(\underline{r}, \underline{r}_1) \text{Im}\{\mu_{zz}(\underline{r}_1)\} G_{zz}^{HH*}(\underline{r}, \underline{r}_1) \\ &+ \frac{\omega \mathcal{E}_0}{\pi} \theta(\omega, T) \int d^2 r_2 \sum_{n=x,y} \sum_{m=x,y} G_{xn}^{EE}(\underline{r}, \underline{r}_2) \text{Im}\{\varepsilon^{mn}(\underline{r}_2)\} G_{zm}^{HE*}(\underline{r}, \underline{r}_2). \end{aligned} \quad (26)$$

the TE polarization of Eq. (19) can be treated in a similar way, that is:

$$E_z(\underline{r}) = \int G_{zz}^{EE}(\underline{r}, \underline{r}_1) J_z(\underline{r}_1) d^2 r_1 + \int G_{zx}^{EH}(\underline{r}, \underline{r}_2) K_T^x(\underline{r}_2) d^2 r_2 + \int G_{zy}^{EH}(\underline{r}, \underline{r}_3) K_T^y(\underline{r}_3) d^2 r_3. \quad (27)$$

$$\underline{H}_n(\underline{r}) = \int G_{nz}^{HE}(\underline{r}, \underline{r}_4) J_z(\underline{r}_4) d^2 r_4 + \int G_{nx}^{HH}(\underline{r}, \underline{r}_5) K_T^x(\underline{r}_5) d^2 r_5 + \int G_{ny}^{HH}(\underline{r}, \underline{r}_6) K_T^y(\underline{r}_6) d^2 r_6. \quad (28)$$

this yields the Poynting vector as:

$$\langle \underline{S}^{TE} \rangle = -2\bar{x} \text{Re}\langle \{E_z H_y^*\} \rangle + 2\bar{y} \text{Re}\langle \{E_z H_x^*\} \rangle = \bar{x} \langle S_x^{TE} \rangle + \bar{y} \langle S_y^{TE} \rangle. \quad (29)$$

$$\begin{aligned} \langle E_z H_y^* \rangle &= \frac{\omega \mathcal{E}_0}{\pi} \theta(\omega, T) \int d^2 r_1 G_{yz}^{EE}(\underline{r}, \underline{r}_1) \text{Im}\{\varepsilon_{zz}(\underline{r}_1)\} G_{yz}^{HE*}(\underline{r}, \underline{r}_1) \\ &+ \frac{\omega \mu_0}{\pi} \theta(\omega, T) \int d^2 r_2 \sum_{n=x,y} \sum_{m=x,y} G_{zn}^{EH}(\underline{r}, \underline{r}_2) \text{Im}\{\mu^{mn}(\underline{r}_2)\} G_{ym}^{HH*}(\underline{r}, \underline{r}_2). \end{aligned} \quad (30)$$

and similarly, for the y-component:

$$\begin{aligned} \langle E_z H_x^* \rangle &= \frac{\omega \mathcal{E}_0}{\pi} \theta(\omega, T) \int d^2 r_1 G_{xz}^{EE}(\underline{r}, \underline{r}_1) \text{Im}\{\varepsilon_{zz}(\underline{r}_1)\} G_{xz}^{HE*}(\underline{r}, \underline{r}_1) \\ &+ \frac{\omega \mu_0}{\pi} \theta(\omega, T) \int d^2 r_2 \sum_{n=x,y} \sum_{m=x,y} G_{zn}^{EH}(\underline{r}, \underline{r}_2) \text{Im}\{\mu^{mn}(\underline{r}_2)\} G_{xm}^{HH*}(\underline{r}, \underline{r}_2). \end{aligned} \quad (31)$$

note that calculations can be repeated for the TE and TM physical spaces. All Green functions were numerically determined. Finally, we notice in all cases that the Poynting flux only depends on the currents correlation, which allows to finalize its calculation without any knowledge of phase currents.

Appendix C: numerical implementation

In this appendix, we briefly summarize the numerical procedures that we used to perform the final calculation. Due to the stochastic nature of thermal radiation, we took account only for the time averaged Poynting vector of the emitted field $\langle \underline{S} \rangle$ defined in Eqs. (21, 24 and 29). In order to perform the calculation of $\langle \underline{S} \rangle$ in the physical space, a triangular mesh was created such that it spans the thermally radiating object; then we calculated the location of each unit cell and its area Δa_i indexed with $i = 1, \dots, L$, where L is the total number of cells. For the virtual space, instead of creating another mesh, the simplest implementation is to transform the mesh created for the emitter in the physical space in such a way that the area of the unit

cell after transformation becomes $\Delta a_i' = \Delta a_i |A|$. The summation in (24, 26, 30 and 31) is done while sweeping over the centroids of the cells such that for each loop, a point current source is in a centroid. To evaluate the Green functions defined in (22, 23, 27 and 28), we have used COMSOL Multiphysics with general PDE modules for full wave simulations as follows:

$$\nabla \cdot (-\underline{c} \circ \nabla u + \underline{\gamma}) + au = f.$$

This module was used to solve the TM differential Eqs. (16-17) and the TE differential Eqs. (19-20). For the TM case of Eq. (16):

$$\underline{c} = \frac{-\underline{\epsilon}_{\equiv T}}{|\underline{\epsilon}_{\equiv T}|}, \underline{\gamma} = \frac{1}{|\underline{\epsilon}_{\equiv T}|} \begin{pmatrix} -\epsilon_{xy} J_T^x + \epsilon_{xx} J_T^y \\ -\epsilon_{yx} J_T^x + \epsilon_{yy} J_T^y \end{pmatrix}, a = k_0^2 \mu_{zz} \text{ and } f = i\omega \epsilon_0 K_z.$$

while for the TE case of Eq. (19)

$$\underline{c} = \frac{-\underline{\mu}_{\equiv T}}{|\underline{\mu}_{\equiv T}|}, \underline{\gamma} = \frac{1}{|\underline{\mu}_{\equiv T}|} \begin{pmatrix} \mu_{xy} K_T^x - \mu_{xx} K_T^y \\ \mu_{yx} K_T^x - \mu_{yy} K_T^y \end{pmatrix}, a = k_0^2 \epsilon_{zz} \text{ and } f = i\omega \mu_0 J_z.$$

Funding

French National Agency of Research (ANR) through the funding of project INPACT (# ANR-13-BS03-0009).